Transverse-field-induced effects in carbon nanotubes

Wade DeGottardi,[1] Tzu-Chieh Wei,[2] and Smitha Vishveshwara[1]
[1]*Department of Physics, University of Illinois at Urbana-Champaign, 1110 West Green Street, Urbana, Illinois 61801-3080, USA*
[2]*Department of Physics and Astronomy and Institute for Quantum Computing, University of Waterloo, 200 University Avenue West, Ontario, Canada N2L 3G1*

(Received 29 December 2008; revised manuscript received 28 April 2009; published 21 May 2009)

We investigate the properties of conduction electrons in single-walled armchair carbon nanotubes in the presence of both transverse electric and magnetic fields. We find that these fields provide a controlled means of tuning low-energy band-structure properties such as inducing gaps in the spectrum, breaking various symmetries, and altering the Fermi velocities. We show that the fields can strongly affect electron-electron interactions yielding tunable Luttinger-liquid physics, the possibility of spin-charge-band separation, and a competition between spin-density-wave and charge-density-wave orders. For short tubes, the fields can alter boundary conditions and associated single-particle level spacings as well as quantum dot behavior.

DOI: 10.1103/PhysRevB.79.205421 PACS number(s): 71.10.Pm, 71.20.Tx

I. INTRODUCTION

The astounding range of experimental and theoretical studies performed on carbon nanotubes[1,2] has revealed a spectrum of physics characteristic of strongly correlated low-dimensional electronic systems.[3] The underlying graphene lattice structure of these tubes uniquely affects band structure, effective dimensionality, Coulomb interaction effects, and the quantum dot behavior exhibited by short nanotube segments. The band structure shows differing behavior depending on various factors such as chirality, applied gate potentials, boundary conditions at the tube ends, and mechanical stress.[4,5] In single-walled armchair nanotubes (SWNT),[6] the entities of interest here, gapless linearly dispersing modes endow the nanotube with its peculiar quantum wire properties. As described theoretically and ascertained experimentally, interactions within the modes of this effectively one-dimensional (1D) system cause it to behave as a Luttinger liquid characterized by non-Ohmic conductances.[3,7–10] Tubes placed between tunnel barriers act as quantum dots,[11,12] which, while displaying zero-dimensional physics such as Coulomb-blockade behavior, retain some higher dimensional traits such as hosting plasmons typical of one dimension and band degrees of freedom attributed to the underlying graphene lattice. Potentially invaluable to applications, these nanotube quantum dots have been proposed as elements of quantum devices and the quantum states of blockaded electrons have been regarded as candidates for units of quantum information.[13] In each of these aspects, the presence of applied fields can dramatically alter the nanotube's behavior; here we present an extensive study of the effects of electric and magnetic fields applied transversally to the axis of the nanotube.

At the level of the band structure, it has been shown that a parallel magnetic field can have the striking effect of converting a metallic tube to a semiconducting one by way of inducing a gap,[14] and vice versa, an effect discernible in conductance, Coulomb-blockade, and scanning tunneling microscope (STM) measurements. Here, instead of a parallel field, we discuss transverse field configurations (both electric and magnetic) and the conditions under which a band gap opens up or the spectrum remains gapless in armchair SWNTs. In the latter case, we demonstrate, via band-structure calculations, simultaneous breaking of the valley degeneracy (of the two distinct Dirac points), the left-right-mover degeneracy, and the particle-hole symmetry. Moreover, the fields yield a non-negligible reduction in the Fermi velocity of conduction electrons traveling along the tube. We show that, for certain configurations of fields, the ground state of the tube can even be made to carry finite current.

Transverse fields provide an excellent means of altering the ratio of interaction strength to the Fermi energy in SWNTs. This makes nanotubes potentially the only systems to date in which the associated Luttinger-liquid physics can be tuned in a controlled fashion. As described in previous work, either an electric field[15] or a magnetic field[16,17] alone suffices to change the value of the Luttinger-liquid parameter from that measured in field-free environments. The magnitude of the electric fields required to bring about a significant change are well within current experimental reach.[18] Here, we find that our approach reproduces these results. We show that such a tuning of Luttinger parameters can mediate a transition from the system showing tendencies toward spin-density-wave (SDW) ordering to that of charge-density-wave (CDW) ordering. Furthermore, in addition to the tuning of the Luttinger parameter presented in previous works for the net charge density,[15–17] we find that Luttinger-type interactions become manifest in modes associated with the density differences between nanotube bands as well. Thus we predict that, akin to spin-charge separation, transverse fields can induce a spin-charge-band separation wherein the three degrees of freedom move at different velocities.

The above results are discussed in the case of an infinite system. For short tubes or finite length segments formed by tunnel barriers, boundary effects need to be taken into account. We find that applied fields influence multiple aspects of short nanotubes. First, fields can alter the single-particle energy-level spacing of the tube. Here, we carefully account for the effect of the tube ends in the case that the left and right movers travel at different speeds. Second, the charging energies become field dependent, and third, the plasmon spectrum varies in accordance with the first two effects. We have conducted a comprehensive analysis of the short nano-

tube as a finite-sized Luttinger liquid and show how all three effects can be captured. Within this description, we discuss the structure of field-dependent Coulomb-blockade peaks, and how the presence of both electric and magnetic fields acts as a means of manipulating quantum states of the dot (the effect of a magnetic field alone has recently been discussed by Bellucci and Onorato[19]).

The present work combines several commonly used theoretical tools in studying field-induced effects. First, we conduct a detailed analysis of SWNT band structure in the presence of transverse electric and magnetic fields. This approach differs from that of Refs. 15–17 and 19 in that we derive the low-energy spectrum directly from the tight-binding model rather than starting with the Dirac equation and its linear spectrum as an input. Hence our approach in calculating the band structure is similar to that presented in Ref. 20 in which the effects of a transverse magnetic field were examined. This more involved approach has the advantage of tracking the field-induced shift in Fermi momentum which turns out to have important implications for quantum dot physics. Our band-structure calculation is then used as an input for a detailed Luttinger-liquid calculation, similar in spirit to Refs. 8 and 19. Thus, we derive an effective one-dimensional description of the field-induced effects in terms of quadratic terms in the Hamiltonian which involve charge current and the charging asymmetry between the two Fermi points. We find that this Luttinger-liquid description provides a natural framework in which to discuss quantum dot physics. A similar calculation in the absence of fields can be found in Ref. 7. Here, in addition to the Luttinger analysis, we account for a wide range of boundary conditions that give rise to different Coulomb-blockade landscapes.

The outline of this paper is as follows. In Sec. II we present the formulation and results of our band-structure calculation. In Sec. III we formulate an effective one-dimensional Hamiltonian which takes into account field effects. We bosonize this Hamiltonian, describing interaction effects in terms of Luttinger-liquid physics. In Sec. IV we investigate the various Luttinger-liquid phases and the feasibility of using fields to access such phases. In Sec. V we discuss field-tuned quantum dot physics. Finally, in Sec. VI we present the highlights of our results and discuss their relevance to experiments.

II. BAND STRUCTURE IN TRANSVERSE FIELDS

We briefly recapitulate the band structure of an infinitely long armchair tube in the absence of any fields.[5] The electronic properties of graphene are well described by a tight-binding model in which electrons hop between nearest neighbors of the underlying hexagonal bipartite lattice (sublattices here are labeled A and B) with an associated energy (the hopping integral) of $t \approx 3$ eV. An armchair carbon nanotube can be regarded as a sheet of graphene rolled along the (n,n) direction (for notation of the chirality, see, e.g., Ref. 5), denoted by $\hat{s}$. This gives rise to states of quantized momentum $k_s=[0,2\pi/L,\ldots,2\pi(2n-1)/L]$, where $L=\sqrt{3}na$ is the circumference of the tube, and $a=\sqrt{3}a_c$, where $a_c \approx 0.142$ nm is the nearest carbon-carbon distance. The resulting series of one-dimensional bands can be described by the wave vectors $\vec{k}=(k_x,\frac{2\pi\ell}{L})$, where k_x is the quasimomentum parallel to the tube's axis and $\hbar\ell$ is the state's angular momentum about the tube's circumference. A convenient set of basis states is given by the following linear combination of atomic orbitals

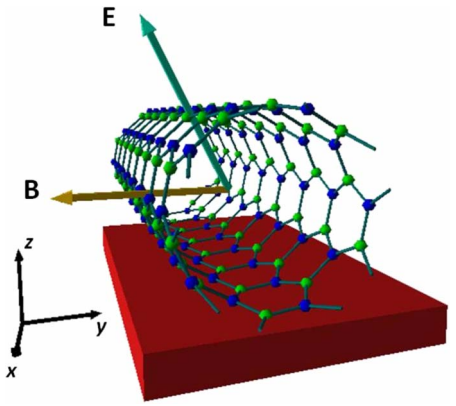

FIG. 1. (Color online) A (5,5) carbon nanotube in the presence of transverse magnetic (pointing in the $-\hat{y}$) and electric fields. The carbon atoms belonging to the A and B sublattices are indicated by dark (blue) and light (green) shading, respectively.

$$|\Phi^{\ell}_{A/B}\rangle = \frac{1}{\sqrt{2n}} \sum_{\vec{R}\in A/B} e^{i\vec{k}\cdot\vec{R}} |\vec{R}\rangle, \tag{1}$$

where $|\vec{R}\rangle$ is the π-electronic state of the atom located at $\vec{R}$. The sum runs over the n atoms in the unit cell that belong to either the A or B sublattice. At half filling, the associated dispersion has low-energy excitations near the so-called Dirac points of the form $\epsilon = \pm\hbar v_F|k-\alpha k_F|$, where $v_F=\frac{\sqrt{3}ta}{2\hbar} \approx 8\times10^5$ m/s, $k_F=4\pi/3a$, and $\alpha=\pm$. Thus, $k=\alpha k_F$ label the two inequivalent Fermi points.

The setup of interest is shown in Fig. 1. An external magnetic field is applied in the negative y direction; an applied (transverse) electric field makes an angle χ with the magnetic field. These fields give rise to scalar and vector potentials

$$U(s) = |e|ER\cos\left(\frac{s}{R}-\chi\right), \tag{2}$$

$$\vec{A} = -Bz\hat{x}, \tag{3}$$

respectively, where E and B are the electric and magnetic field strengths ($R=L/2\pi$). The x axis runs parallel to the tube's axis and the additional coordinate s measures the circumferential distance starting from the negative y axis (a positive value of s corresponds to a clockwise rotation as one looks along the x axis in the negative direction).

These external potentials are easily accommodated within the tight-binding approach. In Eq. (3) we have selected a gauge that is independent of x and thus k_x remains a good quantum number. The hopping matrix elements in the presence of the fields are given by

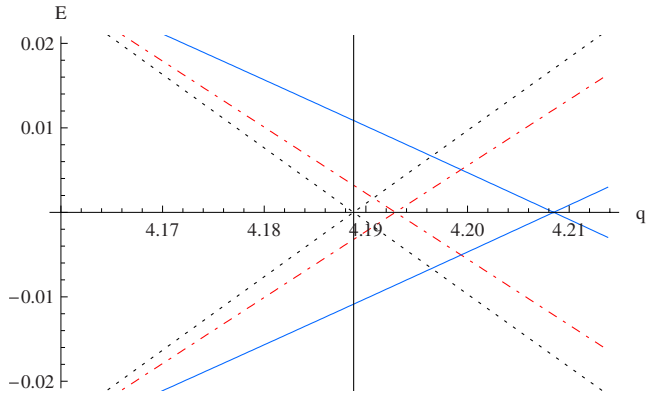

FIG. 2. (Color online) Spectrum of a (5,5) carbon nanotube near the $\alpha=+$ Dirac Fermi point (field-free value $k_F=\alpha 4\pi/3a$ indicated by the vertical line) in the presence of an external transverse electric field with $U_0/t=0$ (black dotted), 0.2 (red dot-dashed), and 0.4 (blue solid) as the crossing moves to the right. The horizontal axis indicates the value of q, where $q=ka$; the vertical axis is given in units of t, the hopping integral ($t\approx 3$ eV).

$$\langle \Phi_A^{\ell'}|H|\Phi_B^{\ell}\rangle = -\frac{t}{2n}\sum_{\vec{R}\in B,\vec{R}'\in A} e^{i(\vec{k}\cdot\vec{R}-\vec{k}'\cdot\vec{R}')+(ie/\hbar)(G_R-G'_R)}, \quad (4)$$

where the sum runs over nearest neighbors $\vec{R}$ and $\vec{R}'$, and

$$G_j - G_i \approx \int_0^1 d\lambda(\vec{r}_i-\vec{r}_j)\cdot\vec{A}[\vec{r}+\lambda(\vec{r}_i-\vec{r}_j)] \quad (5)$$

is the Aharonov-Bohm phase associated with the magnetic field Ref. 5. We have assumed that the hopping integral t is independent of the electric field. The dimensionless parameter b is given by $b=B\frac{\sqrt{3}|e|L^2}{4\pi^2\hbar}$. Numerically, for an (n,n) nanotube, the magnetic field in tesla is related to the dimensionless parameter b via $B\approx 8.1\times 10^4\times b/n^2$ T. The scalar potential gives rise to an on-site potential described by the matrix element,

$$\langle \Phi_A^{\ell'}|H|\Phi_A^{\ell}\rangle = \langle \Phi_B^{\ell'}|H|\Phi_B^{\ell}\rangle = \frac{tU}{2}e^{\pm i\chi}, \quad (6)$$

for $\ell'=\ell\mp 1 \mod n$ where $U=|e|ER/t$. The electric field strength in V/nm is related to U by $E=Ut/|e|R \approx 42U/n$ V/nm for a tube with chiral vector (n,n). That these matrix elements mix states of different angular momentum has a straightforward classical analog: a charged particle on the surface of a cylinder will circulate around the tube's circumference as a result of the applied fields.

We have studied the effects of the fields perturbatively in b and U. In the vicinity of the Fermi points, the left- and right-moving bands are nearly degenerate so care must be taken in applying perturbation theory. The details of this calculation are presented in Appendix A where we carry out perturbation theory to second order. There are three cases of interest that we summarize below. An illustration of these three cases is shown in Figs. 2–5. While some of the effects discussed are rather small for standard SWNTs, we note that our band-structure analysis can be applied to multiwalled nanotubes as well in which case a larger radius yields more pronounced effects.

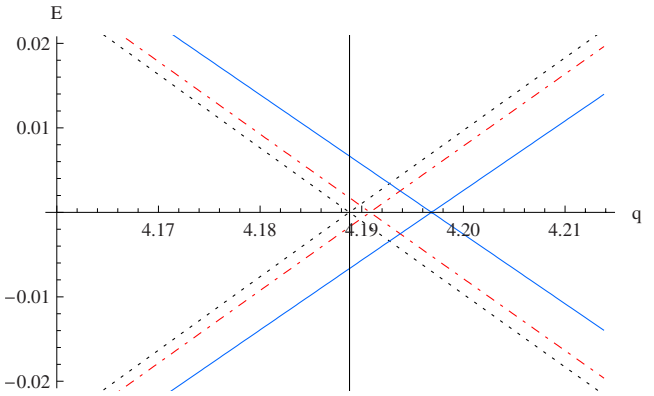

FIG. 3. (Color online) Spectrum of a (5,5) carbon nanotube near the $\alpha=+$ Dirac Fermi point (field-free value $k_F=\alpha 4\pi/3a$ indicated by the vertical line) in the presence of a magnetic field $b=0$ (black dotted), 0.2 (red dot-dashed), and 0.4 (blue solid) (as the crossings move to the right). The horizontal axis indicates the value of q, where $q=ka$; the vertical axis is given in units of t, the hopping integral ($t\approx 3$ eV). While the shift in Fermi point is clear, the change in the slope [cf. Eq. (7)] is small and difficult to discern.

A. Case of $E=0$ or $B=0$

For a single field, the most salient features of our band-structure calculation are the reduction in Fermi velocity and the shift in Fermi momentum. Semiclassically, the reduction in Fermi velocity can be ascribed to the deflection of the electrons by the fields leading to a reduction in the velocity component along the tube. Furthermore the bands remain gapless.

For a magnetic field, we find a reduced Fermi velocity given by

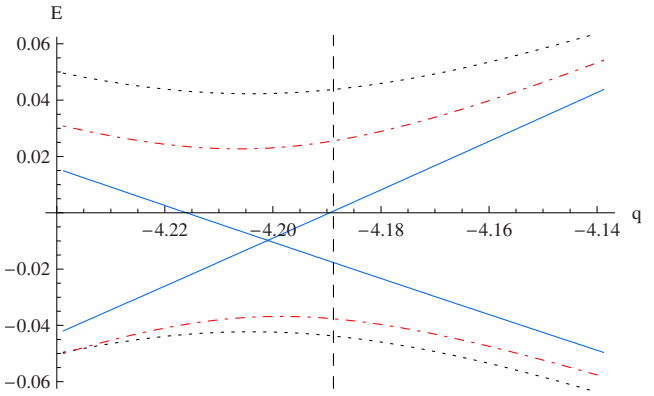

FIG. 4. (Color online) Spectrum of a (5,5) carbon nanotube near $\alpha=-$ Dirac Fermi point (field-free value $\alpha k_F=-4\pi/3a$ indicated by the vertical dashed line) in the presence of transverse electric and magnetic fields ($U/t=0.2$ and $b=0.4$). The angle between $\vec{E}$ and $\vec{B}$ being 0 (black dotted), $\pi/4$ (red dot-dashed), and $\pi/2$ (blue solid) (from outer to inner). The horizontal axis indicates the value of q, where $q=ka$; the vertical axis is given in units of t, the hopping integral ($t\approx 3$ eV).

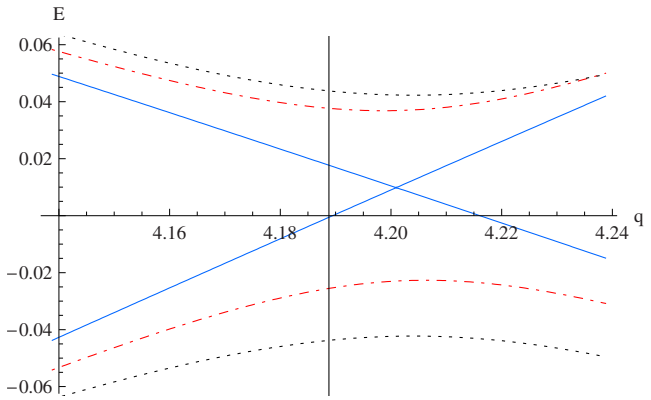

FIG. 5. (Color online) Spectrum of a (5,5) carbon nanotube near $\alpha=+$ Dirac Fermi point (field-free value $\alpha k_F=4\pi/3a$ by the vertical line) in the presence of transverse electric and magnetic fields ($U/t=0.2$ and $b=0.4$). The angle between $\vec{E}$ and $\vec{B}$ being 0 (black dotted), $\pi/4$ (red dot-dashed), and $\pi/2$ (blue solid) (from outer to inner). The horizontal axis indicates the value of q, where $q=ka$; the vertical axis is given in units of t, the hopping integral ($t\approx 3$ eV).

$$\tilde{v}_F = v_F(1 - \Delta v_1 b^2). \tag{7}$$

The first-order correction in b vanishes because $\tilde{v}_F$ must be an even function of b by symmetry. The term Δv_1 is a function of n and is given by Eq. (A4b). This term depends on the geometric details of an armchair tube; for large tubes $\Delta v_1 \approx 1/3$. An experimental observation of such a reduction will require strong fields. For example, a (20,20) armchair tube with a 20 T field gives a 0.4% reduction in the Fermi velocity.

For an electric field we have

$$\tilde{v}_F = v_F(1 - \Delta v_2 U^2). \tag{8}$$

A field of strength 0.1 V/nm corresponds to a reduction in the Fermi velocity of a (10,10) tube of roughly 10%. The term $\Delta v_2 \approx n^2/\pi^2$ for large tubes; its exact form is given by Eq. (A4c).

As mentioned in Sec. I, the reduction in the Fermi velocity has been noted by several authors.[15–17] In these papers the carbon nanotube was modeled as a smooth cylinder and the low-energy electronic behavior was put in by hand. Our results are in agreement with these results in the limit of small fields and large n (in the regime that perturbation is valid). Additionally, by taking into account the geometry of the armchair nanotube, we find that either a magnetic or electric field alone will shift the Fermi points. That is, the nanotube still has the same low-energy spectrum with renormalized values of k_F [whose precise form is given by Eq. (A5)]. The band structure of a (5,5) nanotube in the presence of electric and magnetic fields of various strength is shown in Figs. 2 and 3, respectively.

B. Case of $\vec{E} \perp \vec{B}$ ($\chi=\pi/2$)

Mutually perpendicular fields break both the time-reversal and particle-hole symmetries of the band structure. The left and right movers now move with different speeds. For a magnetic field in the negative y direction and an electric field in the positive z direction, we have

$$\tilde{v}_r = v_F(1 - \Delta v_1 b^2 - \Delta v_2 U^2 \pm \Delta v_3 bU), \tag{9}$$

where r is + for right movers and − for left movers. The expressions for Δv_3 is given by Eq. (A4d); for large tubes $\Delta v_3 \approx n/\pi$. For the fields we consider, E/B is roughly the same order of magnitude as v_F and thus it is natural to expect the band structure will reflect the behavior of a classical velocity selector. Indeed, the asymmetry of the velocity in the right- and left-moving branches is expected from elementary considerations. For a charged particle moving on a smooth cylinder in the presence of mutually perpendicular transverse magnetic and electric fields, the direction of the force caused by the magnetic field depends on the particle's direction of motion, whereas the electric field remains the same. Hence, for fixed kinetic energy, the force in the transverse direction causing the particle to spiral is different for different directions of motion thereby giving rise to different velocities for left and right movers.

Another prominent feature of the band structure in this case is a relative energy shift with respect to the two Fermi points. Near the two Dirac points corresponding to $\alpha = \pm(\alpha k_F \approx \pm \frac{4\pi}{3a})$, we have

$$\epsilon_{r\alpha}(k) = \hbar r \tilde{v}_r(k - \alpha \tilde{k}_F) + \alpha t \Delta s + \mathcal{O}(\Delta k^2). \tag{10}$$

By definition, $\tilde{k}_F$ is the momentum for which the left- and right-moving bands for a given Fermi point are degenerate, and again is generally different from $4\pi/3a$ in the presence of fields. The precise forms of k_F and Δs are given by Eqs. (A5) and (A6), respectively. The solid blue lines in Fig. 4 (for $\alpha=+$) and Fig. 5 ($\alpha=-$) indicate low-energy dispersion of a (5,5) nanotube in the presence of crossed electric ($v=0.2$) and magnetic ($b=0.4$) fields.

C. Case of $\chi \neq \frac{\pi}{2}$

The presence of both electric and magnetic fields will generically open gaps at the Fermi points. The size of this gap is given by

$$\epsilon_{\text{gap}} \approx tbU \frac{2\sqrt{3}\cos\frac{\pi}{3n}}{1 + 2\cos\frac{\pi}{3n}} |\cos\chi|. \tag{11}$$

For example, a (15,15) tube parallel electric and magnetic fields of 1 V/nm and 10 T, respectively, gives $\epsilon_{\text{gap}} \approx 4$ meV. For electric and magnetic fields which are not parallel, this gap is weakly indirect.

The degeneracy associated with the graphene Fermi points stems from the equivalence of the two sublattices. For example, a two-dimensional honeycomb lattice with A and B sublattices composed of different types of atoms would generically have a gap.[5] Now, in a nanotube, gaps can arise for different reasons. For example, the gap associated with a semiconducting tube occurs because the quantized bands miss the Dirac point of the underlying graphene lattice. Such

a gap can be closed by applying a magnetic field (of a specific strength) parallel to the tube's axis. In the present case however, the gap arises from an energy difference associated with the two sublattices and therefore cannot be so closed. Not surprisingly, the gap described here vanishes precisely when the electric and magnetic forces on a classical charged particle traveling along the tube are either parallel or antiparallel.

From Figs. 4 and 5 we clearly see that as the angle between the fields varies, the particle-hole symmetry and the valley degeneracy, as well as the symmetry between left- and right-moving spectra, are broken. The degree of breaking of these symmetries is greatest in the case that the fields are perpendicular. On the other hand, these symmetries are preserved when the fields are parallel or antiparallel and the gap is at its maximum. This angle-dependent gap can be manifested in the transport measurement, e.g., the conductance can be $4e^2/h$, $2e^2/h$, or zero, depending on whether there are four, two, or zero conducting channels (including spin).

D. Low-energy modes

In order to study the low-energy physics of electronic excitations about the Fermi energy for all the cases described above, we can identify the fermionic operator on the cylindrical surface of the tube as approximately

$$\Psi_\sigma(x,s) = \sum_{p\alpha} \varphi_{p\alpha}(x,s)\psi_{p\alpha\sigma}(x), \tag{12}$$

where $\psi_{p\alpha\sigma}(x)$ is the one-dimensional field operator at the point x along the tube axis associated with the A and B sublattices $[p=A(+)/B(-)]$, Fermi points $\alpha k_F=\alpha 4\pi/3a$ $(\alpha=\pm)$, and spin $\sigma=\uparrow(+)/\downarrow(-)$. The Bloch wave function $\varphi_{p\alpha}(x,s)$ retains detailed information about the response of the electronic wave functions to the applied fields.[7,8] While the sublattice basis (indexed by p) is convenient for discussing these wave functions, it does not diagonalize the hopping interaction. We therefore transform to the right- and left-moving bases $[r=R(+)/L(-)]$ via the transformation $\psi_{p\alpha\sigma}=\Sigma_r U_{pr}\psi_{r\alpha\sigma}$, where $U^\dagger\sigma_y U=\sigma_z$.[8] This gives a kinetic-energy term

$$H_0 = -i\hbar\sum_{r\alpha}\int dx r v_r \psi^\dagger_{r\alpha}\partial_x\psi_{r\alpha}, \tag{13}$$

where as shown above a generic field configuration can give rise to the possibility that $v_R\neq v_L$.

The gap which arises as a result of the presence of both electric and magnetic fields [Eq. (11)] can be incorporated into our Hamiltonian by a mass term

$$H_{\text{gap1}} = \sum_{r\alpha\sigma}\int dx \frac{\epsilon_{\text{gap}}}{2}\psi^\dagger_{r\alpha\sigma}\psi_{-r\alpha\sigma}. \tag{14}$$

Note that this mass term is of a different form than that considered in the exhaustive zero-field study by Egger and Gogolin[8] (which had the form $i\frac{\epsilon_{\text{gap}}}{2}r\psi^\dagger_{r\alpha\sigma}\psi_{-r\alpha\sigma}$). Similarly, the effect of the shift associated with the Fermi points can be described by the term

$$H_{\text{gap2}} = \sum_{r\alpha\sigma}\int dx \alpha\frac{t\Delta s}{2}\psi^\dagger_{r\alpha\sigma}\psi_{r\alpha\sigma}. \tag{15}$$

While these gaps are a result of band-structure effects, it is expected that the dominant gap producing effect would be due to electron-electron interactions, partially describable within the Luttinger-liquid formulation of the following section. Such gaps, attributed to Mott insulating behavior, have been recently observed in a dramatic fashion.[21]

III. LUTTINGER LIQUID FORMULATION

In this section we specialize to the case of gapless modes for which interactions can be easily incorporated. As the simplest case, when only a magnetic or electric field is present, the kinetic piece of the Hamiltonian given in Eq. (13) now has $\tilde{v}_+=\tilde{v}_-\equiv\tilde{v}_F$ and $\epsilon_{\text{gap}}=0$, i.e.,

$$H_0 = -i\hbar\tilde{v}_F\sum_{r\alpha\sigma}\int dx \psi^\dagger_{r\alpha\sigma}\partial_x\psi_{r\alpha\sigma}. \tag{16}$$

We use standard approaches such as bosonization to study the effect of fields. Where appropriate, we include discussions for the asymmetric case of $\tilde{v}_+\neq\tilde{v}_-$. We closely follow the approach of Ref. 8 whose lucid pedagogical exposition we do not repeat but instead confine our discussion to the new field-dependent features.

The presence of fields does not alter the fact that the electrons on a tube are locked into their lowest energy radial mode. Hence, it is possible to study the low-energy excitations in the presence of interactions using an effective bosonized 1D Hamiltonian. Bosonization offers great simplification since many of the quartic interaction terms in the fermionic language become quadratic once they are bosonized.

The interaction term takes the general form

$$H_{\text{int}} = \frac{1}{2}\int d\mathbf{r}\int d\mathbf{r}'\Psi^\dagger_\sigma(\mathbf{r})\Psi^\dagger_{\sigma'}(\mathbf{r}')U(\mathbf{r}-\mathbf{r}')\Psi_{\sigma'}(\mathbf{r}')\Psi_\sigma(\mathbf{r}), \tag{17}$$

where $\Psi_\sigma(\mathbf{r})$ is the field in Eq. (12) describing low-energy electrons.

Following Ref. 8, we employ the form of the Coulomb interaction on the surface of a cylinder given by

$$U(x-x',s-s') = \frac{e^2/\kappa}{\sqrt{(x-x')^2+4R^2\sin^2\left(\frac{s-s'}{2R}\right)+a_z^2}}, \tag{18}$$

where R is the radius of the tube, x and s are the coordinates defined in the previous section, and $a_z\approx a$ is roughly the thickness of the graphene sheet.[8] The form of the interaction in Eq. (17) is explicitly given in terms of two-dimensional integrals. An effective interaction term involving purely linear integrals along the tube's axis can be obtained by expressing $\Psi_\sigma(\mathbf{r})$ in terms of the linear and circumferential fields as in Eq. (12), and integrating out the circumferential

degrees of freedom from Eq. (17). Integration over the circumferential degrees of freedom generates quadratic terms absent in the field free case.

The resulting effective interaction involves two-particle scattering processes between fermions moving along the tube axis denoted by the fields $\psi_{r\alpha\sigma}$. The associated scattering processes can be classified according to whether the incoming particles preserve their Fermi-point quantum number α when scattered—forward scattering (αFS)—or scatter across the Fermi surface—backscattering (αBS). In Ref. 8, a further distinction is made in the forward-scattering events depending on whether the interaction potential is homogeneous over the circumference of the tube ($\alpha FS0$) or is able to distinguish the microscopic differences which arise between sublattices ($\alpha FS1$). At this point, in order to obtain an effective low-energy description of the interacting electrons, the one-dimensional fermionic operators can be bosonized as in Ref. 8:

$$\psi_{r\alpha\sigma} = \frac{\eta_{r\alpha\sigma}}{\sqrt{2\pi a_c}} \exp[i\alpha k_F x + i\varphi_{r\alpha\sigma}], \tag{19}$$

where

$$\varphi_{r\alpha\sigma} = \frac{\sqrt{\pi}}{2}(\phi_{c+} + r\theta_{c+} + \alpha\phi_{c-} + r\alpha\theta_{c-} + \sigma\phi_{s+} + r\sigma\theta_{s+} + \alpha\sigma\phi_{c-} + r\alpha\sigma\theta_{s-}). \tag{20}$$

The bosonic fields φ's satisfy the commutation relations

$$[\varphi_{r\alpha\sigma}(x), \varphi_{r'\alpha'\sigma'}(x')] = -i\pi r\delta_{rr'}\delta_{\alpha\alpha'}\delta_{\sigma\sigma'}\ \mathrm{sgn}(x-x'), \tag{21}$$

where $r=\pm$ denotes the left and right movers, $\alpha=\pm$ indicates the Fermi points, and $\sigma=\pm$ represents the spin direction ($\uparrow/\downarrow$). The $\eta_{r\alpha\sigma}$'s are the so-called Klein factors; they enforce the anticommutation relations between different channels,

$$\{\eta_{r\alpha\sigma}, \eta_{r'\alpha'\sigma'}\} = 2\delta_{rr'}\delta_{\alpha\alpha'}\delta_{\sigma\sigma'}. \tag{22}$$

Moreover, the fields $\theta_{j\delta}(x)$'s (with $j=c/s$ and $\delta=\pm$) and their dual fields $\phi_{j\delta}(x)$ [both are linear combinations of $\varphi_{r\alpha\sigma}(x)$] in turn satisfy

$$[\phi_{j\delta}(x), \theta_{j'\delta'}(x')] = -\frac{i}{2}\delta_{jj'}\delta_{\delta\delta'}\ \mathrm{sgn}(x-x'). \tag{23}$$

The effective density in a given channel takes the form

$$\tilde{\rho}_{r\alpha\sigma}(x) = \frac{r}{2\pi}\partial_x\varphi_{r\alpha\sigma}(x). \tag{24}$$

The kinetic energy associated with the linearly dispersing fermionic modes is quadratic in the bosonized fields. As for the interactions, the dominant contributions also come from quadratic terms reflecting net density-density type interactions. As in the field-free case, the $\alpha FS0$ process has one such contribution from the usual Coulomb form involving the net charge density, which in the bosonized representation is given by

$$H_{\alpha FS,0} = \frac{2}{\pi}\int dx\tilde{V}(k\approx 0)(\partial_x\theta_{c+})^2, \tag{25}$$

where

$$\tilde{V}(k) \approx \frac{2e^2}{\kappa}(|\ln kR| + c_0) \tag{26}$$

is the Fourier transform of $V(x)$ and c_0 is a function of n [see Eq. (B1)].

The presence of either an electric or magnetic field gives rise to additional quadratic terms in the $\alpha FS0$ process. These terms have their origin in the nonzero angular-momentum components of the circumferential wave function $\varphi_{r\alpha}(x,s)$ in Eq. (12). A detailed accounting of the radial-wave functions (see Appendix B) shows that an electric field contributes a term

$$H_{\alpha FS,E} = \int dx\left(\frac{2e^2}{\kappa}\right)\left(\frac{2}{\pi}\right)h_1U^2(\partial_x\phi_{c+})^2, \tag{27}$$

whereas a magnetic field provides a contribution

$$H_{\alpha FS,B} = \int dx\left(\frac{2e^2}{\kappa}\right)\left(\frac{2}{\pi}\right)h_2b^2(\partial_x\theta_{c-})^2. \tag{28}$$

In the presence of mutually perpendicular transverse electric and magnetic fields, there is an additional contribution to the interaction

$$H_{\alpha FS,BE} = \int dx\left(\frac{2e^2}{\kappa}\right)\left(\frac{2}{\pi}\right)h_3Ub(\partial_x\theta_{c-})(\partial_x\phi_{c+}). \tag{29}$$

The values of h_1, h_2, and h_3 are given in Appendix B. The Luttinger-liquid Hamiltonian takes into account all these quadratic terms; other terms emerging from the interaction potential are subdominant and can be considered perturbatively.

An intuitive physical picture for the origin of the field-dependent interaction terms above can be obtained by noting that in Eq. (A7) the charge density for $\rho_{r\alpha}$ is of the approximate form $1+t_1ru\sin\frac{s}{R}+t_2\alpha\cos\frac{s}{R}b$. This is broadly consistent with the magnetic field coupling to momentum via $(p-eA/c)^2$ and hence to αk_F, resulting in a term $\sim\alpha b$. Moreover, the electric potential differs slightly between adjacent A and B sites, and in turn couples to left and right movers differently, resulting in a term $\sim rU$. Equation (17) thus gives rise to interactions among the charge densities $\partial_x\theta_{c\pm}$ and current $\partial\phi_{c+}$. We therefore obtain the following nonvanishing terms: (1) $\partial_x\theta_{c+}$, (2) $\partial_x\theta_{c-}\sim b$, and (3) $\partial_x\phi_{c+}\sim u$. Hence, one expects the resulting interaction terms given above.

The sum of the kinetic energy and interactions described by Eqs. (16), (25), (27), and (28) gives the total Hamiltonian that we focus on in this paper

$$H_{\mathrm{tot}} = H_0 + H_{\alpha FS,0} + H_{\alpha FS,E} + H_{\alpha FS,B}. \tag{30}$$

For the case of a single field (either magnetic or electric) the dispersion remains symmetric and therefore Eq. (30) can be written in the form

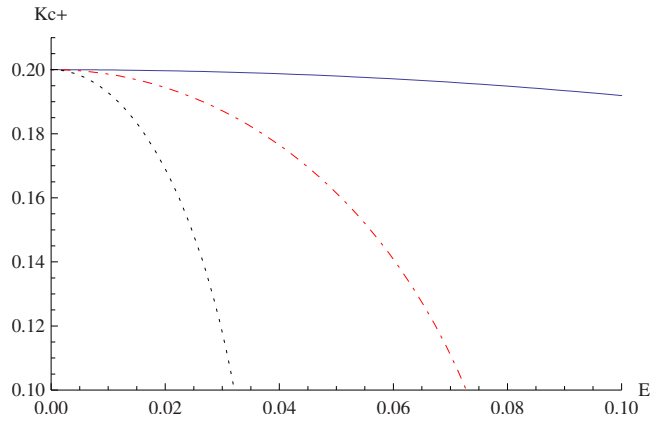

FIG. 6. (Color online) Luttinger parameter K_{c+} of a nanotube as a function of electric field strength E (in V/nm) for different values of n: $n=20$ (solid blue line), $n=40$ (red dot-dashed line), and $n=60$ (black dotted line) (corresponding to tubes of radii of 1.38, 2.75, and 4.13 nm, respectively). The field-free value of the Luttinger parameter is given by $K_{c+}^0=0.2$.

$$H_{\rm tot} = \sum_{a=\pm c/s} \frac{v_a}{2} \int dx \left[\frac{1}{K_a} (\partial_x \theta_a)^2 + K_a (\partial_x \phi_a)^2 \right]. \quad (31)$$

$K_a=1$ reflects no interactions in the "a" sector and $K_a<1$ reflects repulsive interactions. For the asymmetric case, the diagonalization of the Luttinger-liquid Hamiltonian is technically more complicated but conceptually simple given the quadratic form of the relevant terms.[22] Below we discuss the form of the various Luttinger parameters and the related physics.

A. Luttinger parameters for $B=0$, $E\neq 0$

As seen above, for just an electric field present, interactions only affect the net charge sector $c+$ and renormalize the velocity in this sector

$$v_{c+}K_{c+} = \tilde{v}_F + \frac{8e^2 h_1 U^2}{\pi\kappa}, \quad (32)$$

$$v_{c+}/K_{c+} = \tilde{v}_F + \frac{8e^2}{\pi\kappa}(|\ln k_c R| + c_0), \quad (33)$$

where $k_c \approx 1/L$ is the lower cutoff provided by the length L of the tube. This yields a Luttinger parameter value,

$$K_{c+} = \sqrt{\frac{1+\dfrac{8e^2 h_1 U^2}{\pi\kappa\tilde{v}_F(U)}}{1+\dfrac{8e^2}{\pi\kappa\tilde{v}_F(U)}(|\ln k_c R| + c_0)}}, \quad (34)$$

in the low-field limit, where $\tilde{v}_F(U)$ is the field reduced Fermi velocity calculated in the previous section. Figure 6 shows the dependence of K_{c+} on U. In the other sectors, the Luttinger parameters retain their noninteracting value $K_{c-}=K_{s\pm}=1$. The Luttinger model predicts power-law behavior for the tunneling density of states[3] with exponents $\alpha_{\rm end}=(K_{c+}^{-1}-1)/4$ and $\alpha_{\rm bulk}=(K_{c+}+K_{c+}^{-1}-2)/8$ for tunneling into the end or bulk of a tube, respectively.

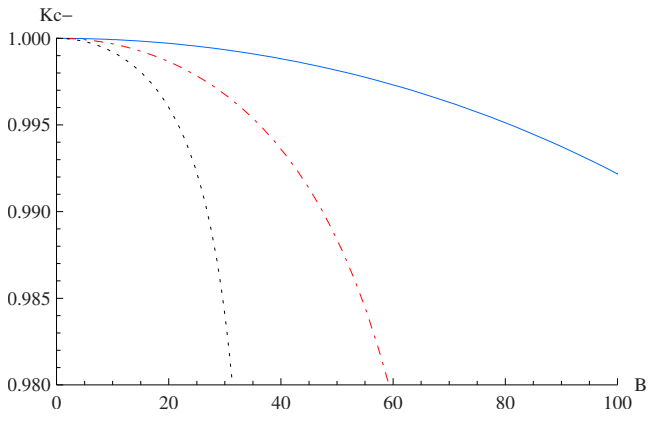

FIG. 7. (Color online) Luttinger parameter K_{c-} of a nanotube as a function of magnetic field strength B (in tesla) for different values of n: $n=20$ (solid blue line), $n=40$ (red dot-dashed line), and $n=60$ (black dotted line).

A smaller value of K_{c+} implies stronger repulsive interactions in the net charge sector. Here, two tendencies compete; in Eq. (34), $\tilde{v}_F(U)<v_F$ increases the interaction strength relative to the kinetic energy. On the other hand, the direct effect of the field, as reflected in the h_1U^2 term in Eq. (34), is to decrease the relative interaction strength. The former effect is dominant of the latter; hence as shown in Fig. 6, K_{c+} is monotonically decreasing in increasing field strength.

B. Luttinger parameters for $B\neq 0$, $E=0$

In the presence of a magnetic field, the Luttinger parameter deviates from the noninteracting value of unity not only in the net charge sector,

$$K_{c+}^{-1} = \sqrt{1+\frac{8e^2}{\pi\kappa\tilde{v}_F(b)}(|\ln k_c R| + c_0)}, \quad (35)$$

but also in the relative charge sector,

$$K_{c-}^{-1} = \sqrt{1+\frac{8e^2 h_2 b^2}{\pi\kappa\tilde{v}_F(b)}}. \quad (36)$$

The spin sectors remain unaffected; $K_{s\pm}=1$.

For both cases $c+$ and $c-$, the reduction in the Fermi velocity $\tilde{v}_F(b)<v_F$ increases the relative interaction strength, thereby decreasing the values of $K_{c\pm}$. In addition, as reflected in the h_2b^2 coefficient in Eq. (36), the field directly decreases K_{c-} via the interaction term of Eq. (28) discussed above. Figure 7 shows the dependence of K_{c-} on the magnetic field B. In this case, the Luttinger model predicts power-law behavior for the tunneling density of states with exponents $\alpha_{\rm end}=(K_{c+}^{-1}+K_{c-}^{-1}-2)/4$ and $\alpha_{\rm bulk}=(K_{c+}+K_{c+}^{-1}+K_{c-}+K_{c-}^{-1}-4)/8$. Unfortunately, this effect is small; even for fields as large as 100 T, K_{c-} is reduced from unity only by about one half of a percent for a (20,20) tube (see Fig. 7). Nevertheless, for multiwalled nanotubes, the outermost layer can have n as large as 100, and hence, the field only needs to be as large as 4 T to see a 0.5% reduction.

The deviation of K_{c-} from unity leads to the fascinating prospect of spin-band-charge separation. In one-dimensional

systems, the possibility of spin-charge separation stemming from different interactions within the two sectors has been extensively discussed and observed in the case of etched quantum wires.[23] Here we predict that nanotubes in transverse magnetic fields can undergo yet another separation due to the interactions in the $c-$ sector. Thus we propose that, in this case, the four modes travel at three different velocities: $v_{c+}=\tilde{v}_F(b)/K_{c+}$, $v_{c-}=\tilde{v}_F(b)/K_{c-}$, and $v_{s\pm}=\tilde{v}_F(b)$.

C. Luttinger parameters for $\vec{E}\perp\vec{B}$

As shown in Fig. 7, the spin-band separation discussed above for purely magnetic fields is a small effect even for very large fields. The prospect of observing this effect is greatly improved for crossed electric and magnetic fields. In this case, the term which mixes the $c+$ and $c-$ sectors is given by Eq. (29) and the values of h_3 are significantly larger than the corresponding terms h_1 and h_2 (see Appendix B). As mentioned previously, the case of crossed fields gives rise to an asymmetric dispersion, and it leads to cross terms $(\partial_x\theta_a)(\partial_x\phi_a)$ with coefficients proportional to the difference v_R-v_L, which is quadratic in the external fields. The full treatment of these and the cross term in Eq. (29) is beyond the scope of the current paper. However, it is possible to get a sense of the order of magnitudes involved by noting that in the present case the dominant field effect is given by Eq. (29). We shall in the following study the effect of this cross term by ignoring the asymmetry in the dispersion. The relevant terms in the Hamiltonian are

$$H=\frac{v_{c+}^0}{2}\int dx\left[\frac{1}{K_{c+}^0}(\partial_x\theta_{c+})^2+K_{c+}^0(\partial_x\phi_{c+})^2\right]+\frac{v_F}{2}\int dx[(\partial_x\theta_{c-})^2+(\partial_x\phi_{c-})^2]+g\int dx(\partial_x\theta_{c-})(\partial_x\phi_{c+}), \tag{37}$$

with $K_{c+}^0=v_F/v_{c+}^0$ defining the field-free values. In diagonalizing the resulting Hamiltonian, care is required to ensure that transformed fields respect commutation relations such as those of Eq. (21). It is straightforward to show that the resulting plasmonic modes retain linear dispersions having associated velocities and Luttinger parameters given by

$$v_\pm^2=\frac{v_F^2}{2}\left\{1+\left(\frac{v_{c+}^0}{v_F}\right)^2\pm\sqrt{\left[\left(\frac{v_{c+}^0}{v_F}\right)^2-1\right]^2+4\left(\frac{gv_{c+}^0}{v_F^2}\right)^2}\right\},$$

$$K_{c\pm}\equiv v_F/v_\pm, \tag{38}$$

where g is the coefficient of the $(\partial_x\theta_{c-})(\partial_x\phi_{c+})$ term and is given by $g=4e^2h_3Ub/\pi\kappa$. The associated tunneling density of states into the bulk of the tube is given by

$$\alpha_{\text{bulk}}=\frac{1}{8}\left(\frac{1}{K_{c+}^0}+K_{c+}^0-2\right)+\frac{1}{4}r\alpha\frac{g}{v_F}+\mathcal{O}(g^2). \tag{39}$$

where r and α indicate the quantum numbers of the electron. This expression differs from the usual form [see the expressions below Eq. (34) and below Eq. (34)] because of the unusual charge-current coupling term in the interactions.

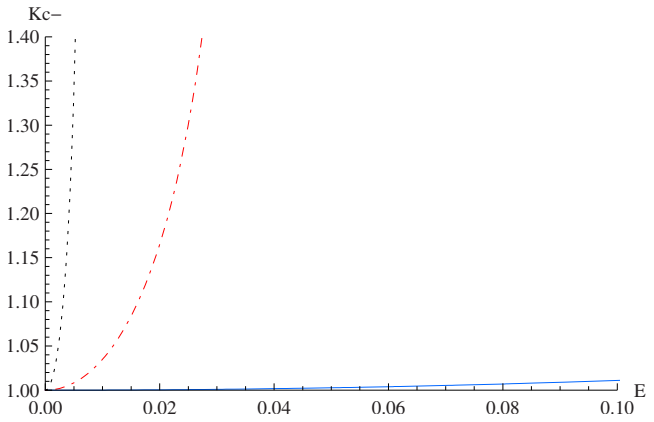

FIG. 8. (Color online) Luttinger parameter K_{c-} of $n=20$ (solid blue line), $n=40$ (red dot-dashed line), and $n=60$ (black dotted line) carbon nanotubes as a function of electric field strength E (in V/nm) in the presence of a 5 T magnetic field (tube has field-free Luttinger parameter $K_{c+}^0=0.2$). See Eq. (38).

Figure 8 shows the dependence of K_{c-} on electric field for a (20,20) nanotube (with $K_{c+}^0=1/5$) in the presence of a 5 T magnetic field. Interestingly, the fields render K_{c-} larger than unity, reflecting tendencies toward perfect conduction in the $c-$ sector. Furthermore, the values attained by K_{c-} show significant deviation from unity, making it feasible to observe the proposed spin-charge-band separation for these field configurations. Figure 9 shows a plot of K_{c+} for the same situation.

IV. LUTTINGER LIQUID PHASES

The field tuning of the Luttinger parameters discussed in the previous section offers a viable way of tuning the ground state of the nanotube through different phases and different ordering tendencies. In the absence of fields, Egger and Gogolin[8] performed an involved analysis using renormalization-group arguments, refermionization, and con-

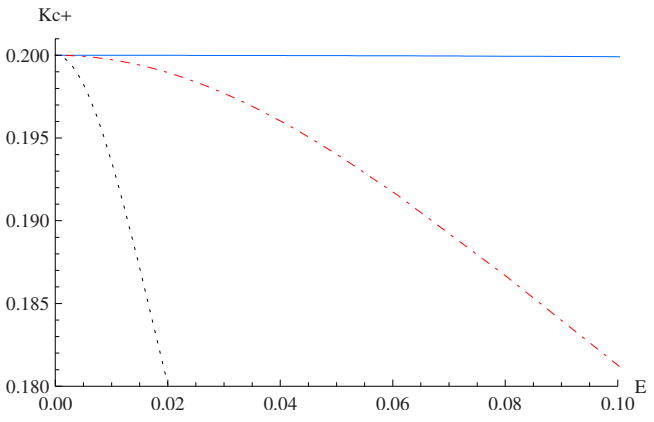

FIG. 9. (Color online) Luttinger parameter K_{c+} of $n=20$ (solid blue line), $n=40$ (red dot-dashed line), and $n=60$ (black dotted line) carbon nanotubes as a function of electric field strength E (in V/nm) in the presence of a 5 T magnetic field (tube has field-free Luttinger parameter $K_{c+}^0=0.2$). See Eq. (38).

siderations of various susceptibilities to predict the ordering tendencies of the nanotube as a function of Luttinger parameters and temperature. In particular, the "Luttinger liquid regime" is the easiest to experimentally access although recent experiments have shown spectacular evidence for gapped Mott insulating behavior.[21] In the Luttinger-liquid regime, wherein all four sectors $c\pm$ and $s\pm$ remain ungapped, the prediction is that, for the range of interaction values $K_{c+}>1/5$, the system tends to show an intersublattice spin-density wave (SDWπ) ordering while for $K_{c+}<1/5$ it tends to show intersublattice charge-density wave (CDWπ) ordering, where the corresponding operators are defined, respectively, as $\hat{O}_{\mathrm{CDW}\pi}\sim\Sigma_{p\alpha\sigma}\psi^{\dagger}_{p\alpha\sigma}\psi_{-p\pm\alpha\sigma}$, and $\hat{O}_{\mathrm{SDW}\pi}\sim\Sigma_{p\alpha\sigma}\sigma\psi^{\dagger}_{p\alpha\sigma}\psi_{-p\pm\alpha\sigma}$. These analyses involved considering operators associated with certain orderings and determining the slowest decaying, equivalently, the most relevant operator (i.e., of the smallest scaling dimension).

Here, we discuss the key changes that occur in the Luttinger regime in the presence of fields. We focus on the Luttinger-liquid regime and consider the manner in which the field-tuned change in Luttinger parameters affect various susceptibilities. We only consider the cases where either only an electric or magnetic field is present; the cases when both fields are present are extremely involved and beyond the scope of this paper. We do not take into account the effect of nonquadratic bosonic terms generated by the fields; even if relevant, we expect that the bare coupling associated with these terms is so small that they only come into play at very low temperatures and not in the Luttinger-liquid regime.

A. Case of $B=0$, $E\neq 0$

For the case of only an electric field present, as discussed above, the effect of the field goes purely into changing the value of K_{c+}. Given that experimentally the value of K_{c+} is around and oftentimes higher than $1/5$, and that the field tends to reduce the value of K_{c+}, the electric field provides a unique means of tuning from a tendency toward (SDWπ) ordering to that of (CDWπ) ordering (see, for example, Fig. 6).

B. Case of $B\neq 0$, $E=0$

The case of only a magnetic field present, as discussed above, presents a slightly more complex situation in which both K_{c+} and K_{c-} deviate from unity. As a result, various susceptibilities acquire a K_{c-} dependence in their scaling behavior. For instance, operators associated with intrasublattice ordering such as $\hat{O}_{\mathrm{CDW0}}\sim\Sigma_{p\alpha\sigma}\psi^{\dagger}_{p\alpha\sigma}\psi_{p-\alpha\sigma}$ and $\hat{O}_{\mathrm{SDW0}}\sim\Sigma_{p\alpha\sigma}\sigma\psi^{\dagger}_{p\alpha\sigma}\psi_{p-\alpha\sigma}$, which in the absence of fields are marginal, both acquire a scaling dimension $(K_{c-}+K_{c-}^{-1}+2)/4$. Tendencies for superconducting order become weaker in the presence of fields; the singlet pairing operator $\hat{O}_{SC0}\sim\Sigma_{p\alpha\sigma}\sigma\psi_{p\alpha\sigma}\psi_{p-\alpha-\sigma}$ acquires the scaling dimension $(K_{c-}+K_{c+}^{-1}+2)/4$.

To determine which ordering dominates, we consider the most relevant candidates: the CDWπ and SDWπ operators, both of which have scaling dimension $(K_{c-}+K_{c+}+2)/4$, parts of the second-order CDWπ operator denoted by $\hat{O}^{2}_{\mathrm{CDW}\pi}$ that have scaling dimension $K_{c-}+K_{c+}$, and a fourth order CDWπ operator denoted by $\hat{O}^{4}_{\mathrm{CDW}\pi}$ which has scaling dimensions $4K_{c+}$. Comparing these exponents shows that $\hat{O}_{\mathrm{CDW}\pi}$ and $\hat{O}_{\mathrm{SDW}\pi}$ are more relevant than $\hat{O}^{4}_{\mathrm{CDW}\pi}$ for $15K_{c+}>2+K_{c-}$, a condition easier to satisfy in the presence of fields than in the field-free case since K_{c-} can then be less than one. Now $\hat{O}^{2}_{\mathrm{CDW}\pi}$ is more relevant than $\hat{O}^{4}_{\mathrm{CDW}\pi}$ for $3K_{c+}>K_{c-}$. For $\hat{O}^{2}_{\mathrm{CDW}\pi}$ to be more relevant than $\hat{O}_{\mathrm{CDW}\pi}$ and $\hat{O}_{\mathrm{SDW}\pi}$ requires $K_{c+}+K_{c-}<2/3$, a condition requiring inaccessibly strong interactions. Finally, to determine whether $\hat{O}_{\mathrm{CDW}\pi}$ or $\hat{O}_{\mathrm{SDW}\pi}$ dominates, we appeal to the arguments of Ref. 8; at lower temperatures where the physics is dominated by certain strong-coupling fixed points, pinning of the θ_{s+} mode suppresses $\hat{O}_{\mathrm{CDW}\pi}$, making its magnitude in the Luttinger phase smaller than that of $\hat{O}_{\mathrm{SDW}\pi}$. Although the methods of refermionization employed to reach this conclusion are no longer valid for arbitrary values of $K_{c-}\neq 1$, the strong-coupling analysis still holds and we believe that a similar conclusion can be reached for the finite magnetic field situation.

To summarize our results, while a detailed analysis and considerations of operators that are not taken into account in Ref. 8 are in order, the most likely scenario is that the nanotube in the Luttinger regime for the $B\neq 0$, $E=0$ case is dominated by SDWπ ordering tendencies for $15K_{c+}>2+K_{c-}$ (the more likely scenario gives that the deviation of K_{c-} from unity is not very large) and CDWπ ordering tendencies for $15K_{c+}<2+K_{c-}$.

V. QUANTUM DOT PHYSICS

For high resistance contacts or sufficiently low temperatures,[3] the nanotube shown in Fig. 1 is only weakly coupled to the leads, thus forming a quantum dot.[24] The behavior of such dots and related Coulomb-blockade effects have been extensively studied by theory and experiment.[7,25] Typical of quantum dot physics, Coulomb-blockade peaks have provided information on single-particle level spacings and charging energies associated with the dot, as well as phase shifts due to scattering at the edges of the nanotube dot. Moreover, under certain conditions, the nanotube quantum dot has revealed a periodicity of four associated with the degeneracy emerging from the band and spin degrees of freedom. Recent work has also investigated the effects of a transverse magnetic field on quantum dot behavior and the associated single-particle and charging energies.[19] Here, we study the role of boundary conditions on nanotube quantum dot physics, which requires subtle considerations in the presence of fields. We then discuss the quantum dot behavior described by a finite-sized version of the nanotube Luttinger-liquid Hamiltonian which takes into account relevant boundary conditions.

A. Field-dependent single-particle energy spectrum

As is well known, finiteness of the tube length leads to a quantized single-particle spectrum which depends on the boundary conditions at the ends of the tube. We assume that the wave functions at a given end are related by

$\psi_{R\alpha\sigma}=\Sigma_{\alpha'\sigma'}M_{\alpha\alpha'\sigma\sigma'}\psi_{L\alpha'\sigma'}$, where M is a matrix which depends on the microscopic details of the tube end but is assumed to be energy independent. We specialize to the case that the boundary conditions do not affect spin; that is, we take $M_{\alpha\alpha'\sigma\sigma'}=S_{\alpha\alpha'}\delta_{\sigma\sigma'}$, where $\delta_{\sigma\sigma'}$ is the Kronecker delta function. We thus assume the absence of magnetic impurities and local moments at the tube ends.

In order to obtain the appropriate boundary conditions for the case of an asymmetric dispersion, we demand that the first quantized kinetic-energy operator $\hat{H}_0=-i\hbar\Sigma_{r\alpha}rv_r\partial_x$ together with the boundary conditions is self-adjoint. This treatment does not account for the effect of interactions on the boundary conditions which would be more naturally discussed in terms of the bosonic fields. Such an analysis shows that there is an additional term in the current proportional to g_2-g_4 which vanishes for the density-density interaction considered here.[26,27] By definition,

$$\langle\Psi,\hat{H}_0\Psi\rangle=-i\hbar\sum_{r\alpha}\int dx r v_r\psi_{r\alpha}^{\dagger}\partial_x\psi_{r\alpha}. \tag{40}$$

Since the boundary effects are assumed to be independent of spin, we have dropped the spin index. For an arbitrary spinor Ψ with $\Psi=(\psi_R\psi_L)^T$, where ψ_R and ψ_L are both two-component spinors in the Fermi-point basis $[\psi_r=(\psi_{r+}\psi_{r-})^T]$, self-adjointness gives

$$\langle\Psi,\hat{H}_0\Psi\rangle=\langle\hat{H}_0\Psi,\Psi\rangle. \tag{41}$$

Integrating the left-hand side of this equation by parts gives

$$\begin{aligned}\langle\Psi,\hat{H}_0\Psi\rangle&=-i\sum_{\alpha=\pm}\int dx(v_R\psi_{R\alpha}^{*}\partial_x\psi_{R\alpha}-v_L\psi_{L\alpha}^{*}\partial_x\psi_{L\alpha})\\&=-i\sum_{\alpha=\pm}[v_R\psi_{R\alpha}^{*}\psi_{R\alpha}-v_L\psi_{L\alpha}^{*}\psi_{L\alpha}]_{x=0,L}+\langle\hat{H}_0\Psi,\Psi\rangle.\end{aligned}$$

Self-adjointness is satisfied as long as the boundary terms vanish, and this leads to

$$\psi_{R\alpha}=S_{\alpha\alpha'}\psi_{L\alpha'}, \tag{42}$$

with $\sqrt{v_R/v_L}S$ unitary.

The details of the S matrix can vary for each experimental setup and depend on physical attributes such as the substrate, the hardness of the confining potential offered by the leads, and the orientation of the tube's sublattices with respect to the leads. These parameters can be incorporated as variables in the boundary conditions which can then be utilized to obtain the single-particle spectrum. The most general version of these boundary conditions are outlined in Ref. 28 via the effective-mass model.

For a given S matrix the spectrum of single-particle states can be determined by applying the condition of Eq. (42) at both ends, and demanding that both the left and right movers have the same energy. The two Fermi points give rise to two sets of bands. The energy between two adjacent states in the *same* band is equal to $\pi\hbar v_H/L$, where v_H is the harmonic mean,

$$v_H=\frac{2v_Rv_L}{v_R+v_L}. \tag{43}$$

However, the energy offset of the bands from the Fermi energy depends on the details of the S matrix. In general, the two Fermi points will give rise to two sets of energy states given by $\pi n\hbar v_H/L+\Delta_1$ and $\pi n\hbar v_H/L+\Delta_2$, where $n\in\mathbb{Z}$.

Since we are ultimately interested in the spacing between Coulomb-blockade peaks, we focus on the energy difference between bands which we define as $\Delta_{\text{band}}=\Delta_1-\Delta_2$ (and for convenience we define Δ_{band} such that $|\Delta_{\text{band}}|<\pi\hbar v_H/L$). We examine two special cases for the S matrix; deriving the Δ_{band} for the most general scattering matrix would be a straightforward extension. First, consider the case in which the tube ends do not mix the Fermi points although we allow the phase shift the electron suffers at the tube end $\delta_{\pm}(x)$ to be different for the two Fermi points ($\alpha=\pm$) and the two tube ends ($x=0,L$). In this case we have $S_{++}(x)=\sqrt{v_L/v_R}e^{i\delta_+(x)}$, $S_{--}(x)=\sqrt{v_L/v_R}e^{i\delta_-(x)}$, and $S_{-+}(x)=S_{+-}(x)=0$. The energy offset between the bands takes the form

$$\Delta_{\text{band}}=\frac{\pi\hbar v_H}{L}\mathcal{F}\left[\frac{\tilde{\delta}_1}{2\pi}+\frac{2t\Delta s}{\hbar\pi v_H/L}\right], \tag{44}$$

where $\tilde{\delta}_1=[\delta_+(L)-\delta_+(0)]-[\delta_-(L)-\delta_-(0)]$ and $\mathcal{F}(x)=x-\lfloor x\rfloor$, with $\lfloor x\rfloor$ as the greatest integer less than or equal to x, and the quantity $t\Delta s$ is the field-induced offset between the two Fermi points as defined in Eq. (10). (See Appendix C for derivation.)

Now, consider an electron that is completely scattered into the opposite Fermi point at both boundaries. For simplicity we take $S_{\alpha\alpha'}(x)=\sqrt{v_L/v_R}e^{i\delta(x)}\delta_{\alpha,-\alpha'}$. In this case, the splitting between bands takes the form

$$\Delta_{\text{band}}=\frac{\pi\hbar v_H}{L}\mathcal{F}\left[\frac{2}{\pi}k_FL+\frac{2t\Delta s}{\pi\hbar v_H/L}\left(\frac{v_R-v_L}{v_R+v_L}\right)\right]. \tag{45}$$

For the limiting case of no fields (this also means that $v_H=v_R=v_L\equiv v_F$), one expects the existence of sets of four single-particle states, namely, two degenerate sets of spin states and two sets of band states whose energy splitting depends on the various phase shifts and the extent to which modes at the two Fermi-point mix. For no Fermi-point mixing, the interband splitting is $\hbar v_F\tilde{\delta}_1/2L$ while for complete Fermi-point mixing, the splitting is $\frac{\pi\hbar v_F}{L}\mathcal{F}[2Lk_F/\pi]$. Coulomb-blockade experiments have shown an interband band splitting of about 10% (Ref. 11) of the $\pi\hbar v_F/L$. Such a persistent approximate degeneracy in band energies for a range of tubes[29] suggests that the magnitude of Fermi-point mixing in these samples is minimal.

B. Tunability of energy subband splitting

As discussed above, the boundary conditions in a given experiment are not directly observable since Δ_{band} depends on several parameters. Fields provide a way of controlling Δ_{band} as well as studying its physical origin in a particular sample. By scanning through various field strengths, the variation in the band offset can reveal information about the

nature of boundary scattering. For example, the extent to which a given tube interpolates between the two expressions given in Eqs. (44) and (45) can be used to determine the importance of (Fermi-point) backscattering at the tube ends. In the case of a *natural* band degeneracy in a tube (that is, no Fermi-point mixing at the ends of the tube and $\tilde{\delta}_1=0$), both electric and magnetic fields need to be applied to break the degeneracy; the magnitude of the subband splitting as a function of fields can be extracted from Eq. (44) by setting $\tilde{\delta}_1=0$. An alternative approach for breaking the subband degeneracy was explored by Ref. 25 in which a nonuniform external potential along the tube was applied. However, this approach becomes infeasible for the case of a diagonal scattering matrix since it relies on band curvature away from half filling.

Thus combining electric and magnetic fields can provide a means of breaking and tuning the degeneracy of the quantum states of electrons inhabiting the nanotube quantum dot. Of the four possible states discussed above, where the direction of spin is defined with respect to the magnetic field, an extra electron would occupy the ground state, which can be chosen to be any of the four depending on the direction of the fields. The quantum state can be characterized by a superspin inhabiting a $SU(2)\otimes SU(2)$ band and spin space. The enhanced control of the spectrum of nanotubes that fields offer would obviously have important implications for any potential quantum information applications.

C. Coulomb-blockade physics

We now consider quantum dot phenomena by taking into account interaction effects in addition to the single-particle level spacing analysis of the previous subsections. To present a coherent picture, we work within the context of the Luttinger-liquid description for field configurations that retain gapless modes. This approach neglects the exchange energy within a dot, which while shown to be present, is often much smaller in magnitude than the level spacing and interaction energy.[11] While our treatment captures salient features of quantum dot behavior, a full analysis of the Luttinger-liquid formulation for the most general boundary conditions is yet to be performed.

Following the method of Ref. 7 (see also Refs. 30 and 31), for a finite-sized version of Eq. (30), we decompose the bosonic fields θ_a and ϕ_a into sums of topological modes θ_a^0, corresponding to a net occupation number of the a sector $N_a=\frac{2}{\sqrt{\pi}}\int_0^L \partial_x \theta_a^0 dx$ and harmonic modes corresponding to plasmons. For simplicity, we consider the case of no Fermi-point scattering so that the Fermi-point basis as defined by Eqs. (20) and (24), and the band basis which diagonalizes the boundary conditions in the previous subsection coincide (and therefore take $a=c/s\pm$). Assuming the boundary conditions derived in the previous section, we integrate out the x dependence for the topological sector in the finite-sized version of Eq. (30). The resulting Hamiltonian associated with "charging energy" for each topological sector takes the form

$$\mathcal{H}_a=\frac{1}{8}\epsilon_a N_a^2, \tag{46}$$

where $\epsilon_a=(\frac{\hbar\pi v_H}{L}+4E_a)$ and E_a is equal to the interaction energy of a given mode. The interaction energy for the net charge sector comes from the forward-scattering contribution of Eq. (25) to yield $E_{c+}\approx\tilde{V}(k)/L$. The contribution due to the electric field given by Eq. (27) is found to be fourth order in fields and can thus be neglected. The magnetic field, however, does contribute to the charging energy; from Eq. (28), it can be shown that $E_{c-}=2e^2h_2b^2/\kappa L$. This expression represents an upper bound that assumes the limit of no Fermi-point mixing.

The topological modes correspond to the addition of charges onto the dot; in addition, plasmon modes that correspond to harmonic vibrations of the densities in the various sectors are present. In principle, the procedure employed in Refs. 7 and 30 to derive the structure of these plasmonic excitations can be generalized to the case of the asymmetric dispersion by incorporating the asymmetric description in Ref. 22. Here we forego such a derivation; most quantum dot experiments involve the adiabatic tuning of parameters such as gate voltage and thus probe purely ground-state properties determined by the topological sectors.

In the presence of a gate voltage V_G, the Hamiltonian associated with the topological modes of the nanotube quantum dot is given by

$$H_L=\sum_{a=\pm c/s}\mathcal{H}_a-\mu N_{c+}+\frac{1}{2}\Delta_{\text{band}}N_{c-}-\Delta_Z N_{s+}, \tag{47}$$

where μ is essentially eV_G and the term $\Delta_Z=\mu_B B$ accounts for the Zeeman splitting. The hierarchy in energy scales can be summarized for a typical tube length of $L=500$ nm. The intrasubband splitting is 3.3 meV. Therefore we have that $\epsilon_{c-}\approx\epsilon_{s+/-}=3.3$ meV. The charging energy is then $\epsilon_{c+}=47.7$ meV. Consider a tube for which the ends of the tube do not appreciably change the Fermi point. In that case the sign of Δ_{band} can be changed by reasonable electric and magnetic field values (for example, this is true for an $n=15$ tube, a 6 T magnetic field, and an electric field of order 1 V/nm). Finally, $\mu_B\approx 0.058$ meV/T and therefore for most situations the Zeeman splitting will be at least an order of magnitude smaller than the other effects considered here.

The Hamiltonian in Eq. (47) forms a starting point for analyzing quantum dot and Coulomb-blockade behavior in short nanotubes. Typically, conductance is measured across the tube as a function of the applied gate voltage V_G and a bias voltage V_B; while for the most part, energetic costs impede the flow of electrons, at special degeneracy points that equally favor an occupation of N and $N+1$ electrons, zero-bias Coulomb-blockade conductance peaks can be observed. Given that the occupation numbers N_a with $a=\{c/s,\pm\}$ are good quantum numbers, the net energy of the system $E_L=\langle H_L\rangle$ for a given configuration of electrons corresponds to a given combination of eigenvalues of N_a. The equilibrium configuration of electrons on the quantum dot can thus be derived by minimization, i.e., by requiring $\frac{\partial E_L}{\partial N_a}=0$ for all N_a sectors, subject to the physical constraint that electron occupation numbers $N_{a=\pm,\sigma=\uparrow/\downarrow}$ take on integer values. The relationship between these two bases is given by $N_{c\pm}=(N_{+\uparrow}+N_{+\downarrow})\pm(N_{-\uparrow}+N_{-\downarrow})$ and $N_{s\pm}=(N_{+\uparrow}-N_{+\downarrow})\pm(N_{-\uparrow}-N_{-\downarrow})$.

As an illustrative example, consider the Coulomb-blockade situation for the simple case of no fields, no band,

or Zeeman splitting ($\Delta_{\text{band}}=\Delta_z=0$ and only the charging energy in the $c+$ sector is nonzero). Applying the condition that $\frac{\partial E_L}{\partial N_a}=0$ gives $\epsilon_{c+}N_{c+}-4\mu=0$ and $N_{c-}=N_{s+}=N_{s-}=0$ (where μ is varied by V_G). These conditions suggest that all the states at a given energy level will fill before filling the subsequent energy level. Now, as the chemical potential is increased, the first extra electron added onto the dot can occupy any of the degenerate states of the $|\alpha=\pm,\sigma=\uparrow/\downarrow\rangle$ space. Suppose that this electron goes in the $\alpha=+$ band with its spin up. The state of the tube is then characterized by the quantum numbers $(N_{c+},N_{c-},N_{s+},N_{s-})=(1,1,1,1)$. Further increasing the chemical potential by an amount E_{c+} will add the next electron to any of the remaining three states. For example, if the filling obeys Hund's rule (i.e., assuming the exchange interaction which we have thus far neglected) then band $\alpha=-$ would be filled with spin-up electron thus giving the state (2,0,2,0). An additional third electron can occupy $+\downarrow$ or $-\downarrow$ state. The energy cost for adding each of these extra electrons is E_{c+}, reflecting the Coulomb charging energy. However, the fifth extra electron requires a chemical-potential increase of $\frac{\pi\hbar v_H}{L}+E_{c+}$, reflecting the Coulomb energy as well as the excitation energy required to occupy the next energy level. This analysis, executed within the Luttinger-liquid description, reproduces the periodicity of four observed in experiment.[11]

In the presence of fields and intrinsic subband splitting, an analysis similar to the one above can be performed for altered values of ϵ and K_a's, and the orders of magnitude discussed after Eq. (47). We take $\Delta_Z\approx 0$ and $\Delta_{\text{band}}>0$. Furthermore, suppose that for a given tube that a nonzero magnetic field gave $E_{c-}<\Delta_{\text{band}}/2$. In that case, the tendency to minimize N_{c-} would give rise to a shell filling opposite to the usual Hund-type filling. For example, the order in which states are filled could take the form $-\uparrow,-\downarrow,+\uparrow,+\downarrow$ or equivalently $(1,-1,1,-1)\rightarrow(2,-2,0,0)\rightarrow(3,-1,1,1)\rightarrow(4,0,0,0)$. Instead of the Coulomb-blockade peaks being of periodicity of four with spacings given by $E_{c+},E_{c+},E_{c+},E_{c+}+\pi\hbar v_H/L$, spacings become $E_{c+}+E_{c-},E_{c+}-3E_{c-}+\Delta_{\text{band}},E_{c+}+E_{c-},E_{c+}+E_{c-}+\pi\hbar v_H/L-\Delta_{\text{band}}$.

The effect of shell filling in nanotube quantum dots has been investigated experimentally by Liang *et al.*[11] The four-electron periodicity was clearly observed via transport measurement. Parameters of charging and exchange energies were determined. The above results, including field-dependent Luttinger parameters, the effect of boundary conditions, the band splitting, asymmetric dispersions, and additional two-electron periodicity can thus be studied in a similar setup with transverse fields. Additionally, the Fabry-Perot transmission resonances in the presence of a transverse magnetic field predicted by Bellucci and Onorato,[19] as well as possible resonances by both transverse electric and magnetic fields (and their relative angles), can be investigated in the same experimental setup. While our arguments here have been confined to adiabatic tuning and zero-bias conductance, our approach can be used to investigate nonequilibrium phenomena, temperature dependences, higher order tunneling events such as cotunneling, and nonadiabatic tuning. Each of these considerations, which is beyond the scope of this paper, would involve excitations of the plasmonic modes.

VI. DISCUSSION; RELEVANCE TO EXPERIMENT

We have investigated the effects of transverse electric and magnetic fields on armchair carbon nanotubes. We found that fields can break several symmetries inherent to the carbon nanotubes—the valley degeneracy, the left-right-mover degeneracy, and the particle-hole symmetry. The magnitude of a gap in the nanotube spectrum can be continuously tuned by varying the strength and the relative angle of the two fields. We also found that the electron-electron interaction is modified by both fields and thus Luttinger-liquid parameters can be tuned by fields. In particular, an interesting consequence is the possibility of spin-charge-band separation. We also discussed how the fields can be used to study boundary effects in finite-sized tubes and to describe the Coulomb-blockade physics in presence of fields.

Each of these salient features can become manifest in experiment, some in dramatic ways. While we summarize these experimental signatures here, details of the physics and orders of magnitude can be found in the relevant section. At the band-structure level, the reduction in the Fermi velocity can be observed by measuring the particle level spacing in a finite-size tube. The shift in the Fermi momentum induced by either field may be detected by virtue of the associated Friedel oscillations around a dopant or impurity using a STM (see, for example, Ref. 32). For both fields present at an arbitrary angle to one another, a continuous conduction gap occurs at the Fermi energy, discernible via direct conductance measurements, shifts in Coulomb-blockade peaks, and STM measurements.[5,10,12] In the transport measurement, the conductance peak can vary from 0 to $2e^2/h$, and to $4e^2/h$, depending on the fields and the chemical potential. Perhaps the most dramatic prediction of band-structure analysis is that an electric and a magnetic field perpendicular to one another, and the tube axis would give rise to a current carrying ground state. Thus, a tube subject to this field configuration placed across two leads should induce a measurable current even in the absence of an applied voltage drop across the leads.

In the regime in which SWNTs exhibit Luttinger-liquid behavior, strong enough fields can give rise to significant changes. The value of the Luttinger parameter associated with the net charge sector can be tuned via either an electric field, a magnetic field, or both. Furthermore, the presence of an electric field gives rise to density-density interactions associated with the difference in densities in the two bands and results in the deviation of the associated Luttinger parameter K_{c-} from its noninteracting value of unity. The tunneling density of states, a quantity ubiquitous to a range of experiments including scanning tunneling microscope studies and conductance measurements,[3,5,9,33] would reflect these changes in its power-law behavior.

As discussed in Sec. IV, changing the Luttinger parameter via fields can result in tuning through phases having charge-density-wave or spin-density-wave orders; such phases are potentially measurable in STM and neutron-scattering experiments. Another exciting prospect comes about in the tuning of K_{c-}, namely, that of spin-band-charge separation. In the past, momentum resolved tunneling experiments have resolved charge and spin modes moving at different velocities

in quantum wires;[23] in principle, a more elaborate version of such an experiment could detect charge, spin, and band modes moving at three different velocities in nanotubes.

In the quantum dot regime, the application of fields acts as a controlled means of changing the Coulomb-blockade structure of the dot, and could potentially have a plethora of applications. For tubes that preserve the fourfold degeneracy emerging from spin and band degrees of freedom in the absence of fields, the presence of fields can serve to break this degeneracy. For tubes that show a lack of degeneracy, fields provide a way of determining the origin of degeneracy breaking. This effect has potential applications to quantum information. Through achieving a desired amount of degeneracy breaking for the four states, fields can be an effective means of initializing the quantum state of an extra electron added on to the dot. Having initialized a quantum state, transitions can be induced to other states. Additionally, as has been demonstrated for semiconducting quantum dot spin states,[34] superpositions can be created by applying oscillating fields. For the energies quoted above, oscillation frequencies would be on the order of 10^{11} Hz.

To conclude, transverse fields induce a rich range of physical effects in the electronic properties of SWNTs from band-structure effects to one-dimensional behavior to quantum dot physics. Several of these features are very much within the reach of current experimental capabilities and are of both fundamental and applied value.

ACKNOWLEDGMENTS

We thank M. Stone for a helpful discussion of the boundary conditions and the condition of self-adjointness in this context. One of us (W.D.) would like to thank Sarang Gopalakrishnan for discussions on the various symmetries of the band structure and Jeremy McMinis for his assistance in preparing the nanotube figure (Fig. 1). This work was supported by the NSF under the Grant No. DMR-0605813 (S.V.,W.D.). T.C.W. was supported by IQC, NSERC, and ORF.

APPENDIX A: BAND-STRUCTURE CALCULATION

In the absence of any fields, the eigenstates of an infinitely long armchair nanotube are superpositions of the states $|\Phi_{A/B}\ell\rangle$ defined by Eq. (1). For the particular case of an armchair nanotube Eq. (4) gives

$$\begin{aligned}\langle \Phi_A^{\ell'}|H_B|\Phi_B^{\ell}\rangle &= -\frac{t}{N}\sum_s e^{i2\pi[(\ell-\ell')s/L]}\Bigg\{e^{i2\pi\ell a/\sqrt{3}L} \\ &+ 2e^{-i2\pi\ell a/2\sqrt{3}L}\cos\Bigg\{\frac{k_y a}{2}+\sqrt{3}B\frac{|e|}{\hbar}\left(\frac{L}{2\pi}\right)^2 \\ &\times\left[\cos\frac{2\pi}{L}s-\cos\frac{2\pi}{L}\left(s-\frac{a}{2\sqrt{3}}\right)\right]\Bigg\}\Bigg\},\end{aligned}$$

where $b=\frac{\sqrt{3}B|e|L^2}{4\pi^2\hbar}$. For small magnetic fields ($b\ll 1$) we have

$$\langle \Phi_A^{\ell'}|H_B|\Phi_B^{\ell}\rangle = tb\,\sin\frac{ka}{2}e^{i\pi\ell/3n}(1-e^{\pm i\pi/3n}) \tag{A1}$$

for $\ell-\ell'=\pm 1 \bmod N$ and

$$\langle \Phi_A^{0}|H_B|\Phi_B^{0}\rangle = tb^2\,\cos\frac{ka}{2}\left(1-\cos\frac{\pi}{3n}\right). \tag{A2}$$

Applying perturbation theory near the Fermi points requires care because of the near degeneracy of the left and right movers. In this case, the usual procedure of first diagonalizing the nearly degenerate subspace fails because the matrix elements within this subspace vanish to the order we are working. However, there are matrix elements for transitions to other energy levels ($\ell\neq 0$) and these matrix elements give rise to an effective interaction between states in the nearly degenerate subspace. The subspace can be diagonalized once these additional interactions are taken into account.[35]

For the gapless case, the low-energy spectrum near half filling is

$$\epsilon_{r\alpha}(k)=\hbar r\tilde{v}_{F,r}(k-\alpha\tilde{k}_F)+\alpha t\Delta s+\mathcal{O}(k^2). \tag{A3}$$

The renormalized Fermi velocity is given by

$$v_r=v_F(1-\Delta v_1 b^2-\Delta v_2 U_y^2\pm\Delta v_3 bU_y), \tag{A4a}$$

where

$$\Delta v_1=\frac{5+4\cos\frac{\pi}{n}}{3\left(1+2\cos\frac{\pi}{3n}\right)^2}, \tag{A4b}$$

$$\Delta v_2=\frac{3+\cos\frac{\pi}{3n}+2\cos\frac{2\pi}{3n}}{12\left(1-\cos\frac{\pi}{n}\right)}, \tag{A4c}$$

$$\Delta v_3=\frac{\left(\cos\frac{\pi}{6n}+\cos\frac{5\pi}{6n}\right)\csc\frac{\pi}{6n}}{\sqrt{3}\left(1+2\cos\frac{\pi}{3n}\right)^2}, \tag{A4d}$$

and

$$\tilde{k}_F=\left[\frac{4\pi}{3a}+\frac{U_y^2}{2\sqrt{3}\left(1+2\cos\frac{\pi}{3n}\right)}+\frac{8}{\sqrt{3}}\sin^2\left(\frac{\pi}{6n}\right)b^2\right]. \tag{A5}$$

The shift between the two Fermi points [see Eq. (10)] is given by

$$\Delta s=\frac{\sqrt{3}\,\sin\frac{\pi}{3n}}{1+2\cos\frac{\pi}{3n}}bU_y. \tag{A6}$$

For the case of mutually perpendicular fields discussed in Sec. II, the electronic densities are given by the vector

$$\rho_{r\alpha}(s) = \frac{1}{2}\begin{bmatrix} 1 + g_1 ru\cos\left(\frac{s}{R}+\frac{\pi}{6n}\right) - g_2 b\alpha\cos\left(\frac{s}{R}+\frac{\pi}{3n}\right) \\ 1 - g_1 ru\cos\left(\frac{s}{R}-\frac{\pi}{6n}\right) + g_2 b\alpha\cos\left(\frac{s}{R}-\frac{\pi}{3n}\right) \end{bmatrix}, \tag{A7}$$

where the upper and lower components are the electronic densities over the A and B sublattices, respectively. The constants g_1 and g_2 are given by

$$g_1 = \frac{1}{2}\csc\frac{\pi}{2n}, \tag{A8}$$

$$g_2 = \sqrt{3}\csc\frac{\pi}{2n}. \tag{A9}$$

APPENDIX B: INTERACTION TERMS

In order to find the form of the effective interaction $V^{rr'}_{\alpha\alpha'}$, we need account for not only the radial dependence of the wave functions but also for the physical separation between the sublattices. Although the factorization performed in Eq. (12) is an approximation, we may still account for the physical separation of the sublattices. We follow the approach introduced in Ref. 8,

$$V^{rr'}_{\alpha\alpha'}(x-x') = \int_0^{2\pi R}\int_0^{2\pi R}\frac{dsds'}{(2\pi R)^2}\times\rho^T_{r\alpha}(s) \times\begin{pmatrix} U(0) & U(a_c) \\ U(-a_c) & U(0)\end{pmatrix}\rho_{r'\alpha'}(s'),$$

where $U(d)$ is a shorthand for the Coulomb interaction with an offset d, that is,

$$U(d) = U(x-x', s-s'+d), \tag{B1}$$

where the right-hand side of this equation is given by Eq. (18).

The constant c_0 which appears in Eq. (26) is given by

$$c_0(n) = -\gamma - \frac{1}{4\pi}\int_0^{2\pi} d\varphi\,\ln\left[\cos^2\frac{\varphi}{2} + \left(\frac{\pi}{\sqrt{3}n}\right)^2\right].$$

Similarly we find that the values of h_1 and h_2 defined in Sec. III are given by (see Table I)

$$h_1(n) = (c_2^2 - c_1^2)f_1(n) + 2c_1c_2f_2(n) + 2(c_1^2+c_2^2)f_3(n),$$

$$h_2(n) = (c_4^2 - c_3^2)f_1(n) + 2c_3c_4f_2(n) + 2(c_3^2+c_4^2)f_3(n),$$

and

$$h_3(n) = 2[(c_1c_3+c_2c_4)f_1(n) + (c_1c_4+c_2c_3)f_2(n) + 2(c_1c_3+c_2c_4)f_3(n)],$$

where

TABLE I. Values of c_0, h_1, h_2, and h_3 for various tube sizes.

n	c_0	h_1	h_2	h_3
5	−0.239	0.491	0.012	3.780
10	−0.064	0.697	0.040	10.370
15	−0.005	0.786	0.020	17.417
20	0.025	0.834	0.122	24.605
25	0.043	0.865	0.008	31.855
40	0.071	0.913	0.003	53.751
60	0.086	0.941	0.002	83.066

$$f_1(n) = \int_{-\pi R}^{\pi R}\frac{dz}{2\pi R}\left\{\ln\left[\cos^2\frac{z-a_c}{2R} + \left(\frac{a_z}{2R}\right)^2\right] + \ln\left[\cos^2\frac{z+a_c}{2R} + \left(\frac{a_z}{2R}\right)^2\right]\right\}\cos\frac{z}{R},$$

$$f_2(n) = \int_{-\pi R}^{\pi R}\frac{dz}{2\pi R}\left\{\ln\left[\cos^2\frac{z-a_c}{2R} + \left(\frac{a_z}{2R}\right)^2\right] - \ln\left[\cos^2\frac{z+a_c}{2R} + \left(\frac{a_z}{2R}\right)^2\right]\right\}\sin\frac{z}{R},$$

$$f_3(n) = \int_{-\pi R}^{\pi R}\frac{dz}{2\pi R}\ln\left[\cos^2\frac{z}{2R} + \left(\frac{a_z}{2R}\right)^2\right],$$

and

$$c_1 = \frac{1}{2}\csc\frac{\pi}{2n}\cos\frac{\pi}{6n},$$

$$c_2 = \frac{1}{2}\csc\frac{\pi}{2n}\sin\frac{\pi}{6n},$$

$$c_3 = \sqrt{3}\csc\frac{\pi}{2n}\sin\frac{\pi}{6n}\cos\frac{\pi}{3n},$$

$$c_4 = \sqrt{3}\csc\frac{\pi}{2n}\sin\frac{\pi}{6n}\sin\frac{\pi}{3n}.$$

APPENDIX C: SINGLE-PARTICLE SPECTRUM WITH BOUNDARY SCATTERING

Here we illustrate the case in which the tube ends do not mix Fermi points; that is, $S_{++}(x)=\sqrt{v_L/v_R}e^{i\delta_+(x)}$, $S_{--}(x)=\sqrt{v_L/v_R}e^{i\delta_-(x)}$, and $S_{-+}(x)=S_{+-}(x)=0$. Assume the wave functions are

$$\psi_R = \begin{pmatrix} Ae^{ik_{R+}x} \\ Be^{ik_{R-}x}\end{pmatrix}, \tag{C1}$$

$$\psi_L = \begin{pmatrix} Ce^{ik_{L+}x} \\ De^{ik_{L-}x} \end{pmatrix}. \quad \text{(C2)}$$

The energy spectrum for each branch is described by Eq. (10), e.g., $\varepsilon_{R,\pm}=\hbar v_R(k_{R\pm}\mp k_F)\pm t\Delta s$. The self-adjointness condition [Eq. (42)] at $x=0,L$ gives

$$\begin{pmatrix} A \\ B \end{pmatrix} = \sqrt{\frac{v_L}{v_R}} \begin{pmatrix} e^{i\delta_+(0)} & 0 \\ 0 & e^{i\delta_-(0)} \end{pmatrix} \begin{pmatrix} C \\ D \end{pmatrix},$$

$$\begin{pmatrix} Ae^{ik_{R+}L} \\ Be^{ik_{R-}L} \end{pmatrix} = \sqrt{\frac{v_L}{v_R}} \begin{pmatrix} e^{i\delta_+(L)} & 0 \\ 0 & e^{i\delta_-(L)} \end{pmatrix} \begin{pmatrix} Ce^{ik_{L+}L} \\ De^{ik_{L-}L} \end{pmatrix}.$$

This gives constraints on the four momenta

$$(k_{R\pm} - k_{L\pm})L = 2\pi n_\pm + \delta_\pm(L) - \delta_\pm(0), \quad \text{(C3)}$$

where $n_\pm$ are arbitrary integers. For the $\alpha=+$ branch, the energy levels corresponding to k_{R+} and k_{L+} should be equal (in order for the wave function to represent an eigenstate). Hence

$$\hbar v_R(k_{R+} - k_F) + t\Delta s = -\hbar v_L(k_{L+} - k_F) + t\Delta s, \quad \text{(C4)}$$

which gives

$$k_{L+} = -k_F - v_R \frac{2\pi n_+ + \delta_+(L) - \delta_+(0)}{(v_R + v_L)L}, \quad \text{(C5)}$$

and thus

$$\epsilon_+(n_+) = \hbar v_H \frac{2\pi n_+ + \delta_+(L) - \delta_+(0)}{2L} + \Delta s, \quad \text{(C6)}$$

where $v_H \equiv 2v_R v_L/(v_R+v_L)$. Similarly, for $\alpha=-$, we have

$$\epsilon_-(n_-) = \hbar v_H \frac{2\pi n_- + \delta_-(L) - \delta_-(0)}{2L} - \Delta s. \quad \text{(C7)}$$

Hence, we arrive at the interband energy difference

$$\Delta_{\text{band}} = \epsilon_+(n_+) - \epsilon_-(n-) = \frac{\pi\hbar v_H}{L}\left(\tilde{n} + \frac{\tilde{\delta}_1}{2\pi} + \frac{2t\Delta s}{\hbar\pi v_H/L}\right),$$

where $\tilde{\delta}_1 = [\delta_+(L) - \delta_+(0)] - [\delta_-(L) - \delta_-(0)]$ and the $\tilde{n}_\pm$ are selected so that $|\Delta_{\text{band}}|$ is less than the intraband spacing. Hence we obtain Eq. (44). A similar consideration leads to Eq. (45).

[1] S. Iijima, Nature (London) **354**, 56 (1991).
[2] J.-C. Charlier, X. Blase, and S. Roche, Rev. Mod. Phys. **79**, 677 (2007).
[3] T. Giamarchi, *Quantum Physics in One Dimension* (Oxford University Press, Oxford, 2004).
[4] H. Ajiki and T. Ando, J. Phys. Soc. Jpn. **65**, 505 (1996).
[5] S. Saito, M. Dresselhaus, and G. Dresselhaus, *Physical Properties of Carbon Nanotubes* (Imperial College Press, London, 1998).
[6] S. Iijima and T. Ichihashi, Nature (London) **363**, 603 (1993); D. S. Bethune, C. H. Klang, M. S. de Vries, G. Gorman, R. Savoy, J. Vazquez, and R. Beyers, *ibid.* **363**, 605 (1993).
[7] C. Kane, L. Balents, and M. P. A. Fisher, Phys. Rev. Lett. **79**, 5086 (1997).
[8] R. Egger and A. O. Gogolin, Eur. Phys. J. B **3**, 281 (1998).
[9] M. Bockrath, D. H. Cobden, J. Lu, A. G. Rinzler, R. E. Smalley, L. Balents, and P. L. McEuen, Nature (London) **397**, 598 (1999).
[10] Z. Yao, H. W. C. Postma, L. Balents, and C. Dekker, Nature (London) **402**, 273 (1999).
[11] W. Liang, M. Bockrath, and H. Park, Phys. Rev. Lett. **88**, 126801 (2002).
[12] U. C. Coskun, T.-C. Wei, S. Vishveshwara, P. M. Goldbart, and A. Bezryadin, Science **304**, 1132 (2004).
[13] S. Sapmaz, P. Jarillo-Herrero, L. P. Kouwenhoven, and H. S. J. van der Zant, Semicond. Sci. Technol. **21**, S52 (2006).
[14] H. Ajiki and T. Ando, J. Phys. Soc. Jpn. **62**, 1255 (1993).
[15] D. S. Novikov and L. S. Levitov, Phys. Rev. Lett. **96**, 036402 (2006).
[16] H.-W. Lee and D. S. Novikov, Phys. Rev. B **68**, 155402 (2003).
[17] S. Bellucci and P. Onorato, Eur. Phys. J. B **47**, 385 (2005); Ann. Phys. **321**, 934 (2006).
[18] N. Mason, private communication, 2008.
[19] S. Bellucci and P. Onorato, Eur. Phys. J. B **52**, 469 (2006).
[20] R. Saito, G. Dresselhaus, and M. S. Dresselhaus, Phys. Rev. B **50**, 14698 (1994).
[21] V. V. Deshpande, Bhupesh Chandra, Robert Caldwell, Dmitry S. Novikov, James Hone, and Marc Bockrath, Science **323**, 106 (2009).
[22] M. Trushin and A. L. Chudnovskiy, Europhys. Lett. **82**, 17008 (2008).
[23] O. Auslaender, A. Yacoby, R. de Picciotto, K. W. Baldwin, L. N. Pfeiffer, and K. W. West, Science **295**, 825 (2002); O. M. Auslaender, H. Steinberg, A. Yacoby, Y. Tserkovnyak, B. I. Halperin, K. W. Baldwin, L. N. Pfeiffer, and K. W. West, *ibid.* **308**, 88 (2005).
[24] M. A. Kastner, Phys. Today **46**(1), 24 (1993).
[25] Y. Oreg, K. Byczuk, and B. I. Halperin, Phys. Rev. Lett. **85**, 365 (2000).
[26] V. I. Fernandez, Ph.D. thesis, Universidad Nacional de La Plata, 2002.
[27] V. I. Fernandez, A. Iucci, and C. M. Naon, Eur. Phys. J. B **30**, 53 (2002).
[28] E. McCann and V. Fal'ko, J. Phys.: Condens. Matter **16**, 2371 (2004).
[29] A. Makarovski, L. An, J. Liu, and G. Finkelstein, Phys. Rev. B **74**, 155431 (2006).
[30] M. Fabrizio and A. O. Gogolin, Phys. Rev. B **51**, 17827 (1995).
[31] S. Eggert, H. Johannesson, and A. Mattsson, Phys. Rev. Lett. **76**, 1505 (1996).
[32] P. T. Sprunger, L. Petersen, E. W. Plummer, E. Laegsgaard, and F. Besenbacher, Science **275**, 1764 (1997).
[33] H. W. C. Postma, M. de Jonge, Z. Yao, and C. Dekker, Phys. Rev. B **62**, R10653 (2000).
[34] F. H. L. Koppens, C. Buizert, K. J. Tielrooij, I. T. Vink, K. C. Nowack, T. Meunier, L. P. Kouwenhoven, and L. M. K. Vandersypen, Nature (London) **442**, 766 (2006).
[35] L. D. Landau and E. M. Lifshitz, *Quantum Mechanics* (Butterworth-Heinemann, Oxford, 1958).